

Adaptive threshold techniques for cognitive radio-based low power wide area network

A.J. Onumanyi¹, A. M. Abu-Mahfouz^{1,2} and G. P. Hancke^{1,3}

¹Department of Electrical, Electronic and Computer Engineering, University of Pretoria, Pretoria, South Africa

²Council for Scientific and Industrial Research, Pretoria, South Africa

³Department of Computer Science, City University of Hong Kong, Hong Kong, China

*Correspondence

A. J. Onumanyi, Department of Electrical, Electronic and Computer Engineering, University of Pretoria, Pretoria, South Africa. Email:adeiza1@futminna.edu.ng

Abstract

Some low power wide area network (LPWAN) developers such as Sigfox, Weightless, and Nwave, have recently commenced the integration of cognitive radio (CR) techniques in their respective LPWAN technologies, generally termed CR-LPWAN systems. Their objective is to overcome specific limitations associated with LPWANs such as spectra congestion and interference, which in turn will improve the performance of many Internet of Things (IoT)-based applications. However, in order to be effective under dynamic sensing conditions, CR-LPWAN systems are typically required to adopt adaptive threshold techniques (ATTs) in order to improve their sensing performance. Consequently, in this article, we have investigated some of these notable ATTs to determine their suitability for CR-LPWAN systems. To accomplish this goal, first, we describe a network architecture and physical layer model suitable for the effective integration of CR in LPWAN. Then, some specific ATTs were investigated following this model based on an experimental setup constructed using the B200 Universal Software Radio Peripheral kit. Several tests were conducted, and our findings suggest that no single ATT was able to perform best under all sensing conditions. Thus, CR-LPWAN developers may be required to select a suitable ATT only based on the specific condition(s) for which the IoT application is designed. Nevertheless, some ATTs such as the forward consecutive mean excision algorithm, the histogram partitioning algorithm and the nonparametric amplitude quantization method achieved noteworthy performances under a broad range of tested conditions. Our findings will be beneficial to developers who may be interested in deploying effective ATTs for CR-LPWAN systems.

1. INTRODUCTION

In recent times, many Internet of Things (IoT)-based applications, for example, smart metering, smart homes, and smart city architectures, depend on different low power wide area network (LPWAN) technologies to guarantee effective communication between end-nodes. LPWAN technologies are suitable for many of these IoT-based applications because they

permit relatively long single-hop communication range at minimal power consumption rates (long battery life-time), low device cost, albeit at low data rates.¹ Nevertheless, since most LPWANs are widely deployed in the relatively congested Industrial, Scientific, and Medical (ISM) band, they are thus prone to problems associated with spectral congestion in the ISM band, such as interference, limited transmission range, and low data rates.² Consequently, many LPWAN developers, for example, Sigfox, Nwave, and Weightless are presently addressing these problems by integrating different cognitive radio (CR) technologies in their respective designs and products.³ For example, Sigfox has integrated CR into some of its base stations and they have connected them to their end servers via an IP-based network.³ Thus, Sigfox networks are presently able to attain very high capacities (now connecting over three million devices) simply by integrating CR techniques in their designs.³

Essentially, CR refers a radio technology that can automatically detect unused channels (white spaces) in a wireless spectrum and then change its transceiver parameters in order to communicate opportunistically, while preventing interference to surrounding primary user (PU) transceivers.^{4,5} Following the IEEE 802.22 standard, CR aims at improving the communication and radio operating behavior of end-nodes within a number of networks, including cellular, WiFi (IEEE 802.15.2), and LPWAN networks. However, our focus in the present article is on the integration of CR in LPWAN.

In this regard, some recent research efforts are noted regarding the effective integration of CR in LPWAN (termed CR-LPWAN). Most of these works were conducted to address specific problems associated with LPWANs such as interference, spectrum underutilization, and limited transmission range. For example, Saifullah et al⁶ developed a new technology called sensor network over white spaces (SNOW), wherein they deployed an innovative physical (PHY) layer design called distributed orthogonal frequency division multiplexing (D-OFDM) to ensure multiple access and bidirectional communication in LPWAN. They extended their work in another article toward improving LPWAN communication over white spaces.⁷ Similarly, Chen et al⁸ introduced cognitive-LPWAN (C-LPWAN) based on an artificial intelligence (AI)-enabled cognitive engine. They suggested that C-LPWAN performs better than some known LPWAN technologies such as LoRa (Long Range), NB-IoT, and LTE-M in terms of its delay reduction and minimal energy consumption rates. The OpenChirp technology was introduced by Dongare et al in Reference 9 as a LPWAN architecture and a gateway (GW) technology integrated with software defined radio (SDR) to explore white spaces. They suggested that their new LPWAN platform offers a cost-effective and highly deployable mechanism, which is based on LoRaWAN technology. In a similar effort, Moon¹⁰ proposed a dynamic spectrum access strategy for CR-LPWAN toward maximizing the spectrum capacity of CR-LPWAN systems. He showed via numerical analysis that CR-LPWAN systems may achieve better blocking probability than existing LPWAN technologies.

The efforts mentioned above regarding CR-LPWAN systems are few; however, they are pioneering since the study of CR-LPWAN systems is only a relatively new and budding area of research. Consequently, it is pertinent to address existing CR-based problems in order to guarantee the effective development of CR-LPWAN systems. Thus, our concern in the present article pertains to the selection of effective adaptive threshold techniques (ATTs) suited for CR-LPWAN systems. It is envisioned that such effective ATTs will be required in most CR-LPWAN technologies, particularly for those that depend on spectrum sensing (SS) in order to identify white spaces. Essentially, an ATT computes an accurate and useful threshold value per input dataset used by a typical CR-LPWAN system to determine whether

a band is free or not for opportunistic communication. If wrong threshold values are estimated by an ATT, then CR-LPWAN systems will be vulnerable to interference, especially toward interfering with close-by cochannel PU transceivers. Furthermore, wrongly estimated threshold values may lead to the underutilization of spectrum by CR-LPWAN systems. Consequently, the development of effective and accurate ATTs has been well studied in the literature; nevertheless, the present article differs by conducting a unique study of different candidate ATTs that may be deployable for CR-LPWAN systems. Prior to the present article, there has been no investigation in this regard, particularly for such an area that contributes greatly to the successful development of CR-LPWAN systems.

The present article contributes in this regard by investigating a CR-LPWAN PHY front-end model, which incorporates the use of ATTs. This objective differentiates the present article from other articles on ATTs. Furthermore, the present article contributes by proposing a PHY layer front-end model for CR-LPWAN systems, which was investigated based on an experimental setup that comprised of the B200 Universal Software Radio Peripheral (USRP) kit. We also investigated different conditions under which some candidate ATTs will either best or least perform in a CR-LPWAN system, while postulating reasons for their respective performances. Indeed, the need for empirical investigations is essential toward supporting potential engineering designs for the effective deployment of CR-LPWAN systems for IoT-based applications. Thus, the contributions of the present article are concisely summarized as follows:

- This article proposes a network architecture suited for the effective deployment of CR-LPWAN systems as well as a PHY layer front-end model that incorporates SS for use in CR-LPWAN systems.
- An experimental setup was constructed to investigate and identify ATTs suited for CR-LPWAN systems. This was achieved based on a USRP device used to model the PHY layer front-end of an emulated CR-LPWAN GW, operated under different spectra conditions.
- We have investigated a broad range of different ATTs including autonomous methods, thus investigating an array of methods that can be deployed for CR-LPWAN systems.

2. RELATED WORK

There are several efforts directed toward developing effective CR-LPWAN systems. For example, Saifullah et al⁶ focused on improving scalability, asynchronous, and bidirectional communication in LPWAN systems. However, with regard to integrating CR in LPWAN, they considered only the use of the geolocation database technology in order to identify white spaces. Nevertheless, they further acknowledged that there is need to integrate SS in CR-LPWAN especially for remote sensing applications. Chen et al in Reference 8 focused on safeguarding critical functions at the network layer, such as reducing delay and energy consumption rates of CR-LPWAN systems. However, in their design, little was mentioned regarding the type of CR sensing technology adopted at the PHY layer. Dongare and Rowe⁹ introduced SDR technology at the LPWAN GW for the future exploration of white spaces. However, they did not mention whether SS was used in their design or not. Moon et al in Reference 10 adopted a centralized sensing mechanism based on SS deployed in a spectrum broker server. He emphasized that CR-LPWAN systems can be distinguished from typical LPWAN systems according to whether SS techniques are used or not. However, Moon did not mention the type of threshold mechanism that was used in his design. With a few of these

works well studied, it is important to note that SS is a fundamental component of an effective CR-LPWAN system, thus, attention must be directed toward the study of ATTs suited for use in CR-LPWAN systems.

In this regard, we have reviewed existing ATTs based on some relevant design factors required for CR-LPWAN systems. Essentially, we expect that an ATT to be deployed in a CR-LPWAN system should possess the following characteristics:

- They must be fully adaptive, that is, they must be independent of the prior knowledge of the noise level or signal-to-noise ratio (SNR) in the band.
- They should be simple and light weight, that is, they should have a time complexity of at least $O(N)$ in order to ensure fast computations as the algorithm's complexity scales as a function of the total number of input samples N .
- Candidate ATTs may need to be fully autonomous, especially if the IoT use-case demands the need for remote and automated capabilities. For example, autonomous capabilities may be required in IoT use-cases where sensing nodes are typically self-reconfigurable such as in military or remote sensing applications.
- They should belong to the class of global-based techniques since a single threshold value is often required in order to detect signals over a broad range of frequencies.

Thus, we reviewed some candidate ATTs that satisfied the above characteristics, such as the forward consecutive mean excision (FCME) algorithm proposed in Reference 11. The FCME algorithm is a simple and effective ATT having a time complexity of $O(N)$. It accepts the input samples and rearranges them in an ascending manner. Then, it uses two finely tuned parameters, namely, the threshold factor and the percentage of clean samples in order to estimate an effective threshold value. The FCME algorithm has been used extensively in different CR technologies and thus considered as suitable to be investigated in our study. The recursive one-sided hypothesis technique (ROHT) presented in References 12 and 13 is a simple and relevant method seemingly suited for investigation. It uses a simple recursive mechanism based on two parameters to estimate effective threshold values. Similar to the FCME algorithm, the ROHT does not depend on prior knowledge of the noise level or SNR in order to estimate effective threshold values, instead it computes a threshold value based only on the input dataset measured per time. We also studied the first-order statistical technique (FOST) introduced by Gorcin et al in Reference 14, which depends only on the mean and SD of the input dataset in order to estimate an effective threshold value. It is the simplest method among the methods considered in our investigation. The histogram partitioning algorithm (HPA) is another simple and effective method proposed in Reference 15. It works by bifurcating the histogram of the input dataset using a threshold factor called the *descent parameter*. The HPA is a global-based method with a time complexity of $O(N)$, thus making it suitable for investigation in our study. We note that the FCME, ROHT, FOST, and HPA algorithms are fully adaptive methods and these algorithms depend on the accurate fine tuning of their respective parameter prior to their use.

Furthermore, we investigated some fully autonomous methods that require no parameter-tuning process for their use, such as the modified Otsu algorithm (MOA),¹⁶ the mean-based HPA (MHPA),¹⁵ and the nonparametric amplitude quantization method (NPAQM).¹⁷ Since these methods are fully autonomous, they may be applied in some specific IoT use-cases, where sensors are required to be self-reconfigurable. These autonomous methods are all simple (ie, they all have a time complexity of $O(N)$), they are global-based methods, and are fully adaptive methods as well, thus making them suitable for investigation in our study.

Furthermore, we acknowledge that there are so many ATTs proposed in the literature such as in References 18-23; however, these methods depend typically on larger parameter sets (ie, >2 parameters). Moreover, although these methods are often effective, nevertheless, they were not considered in our study since they are either too highly parametrized or they often depend on the prior knowledge of the SNR level before they can be used. Unfortunately, these are not the qualities desired of an ATT required for use in a CR-LPWAN system.

3. METHODS

In this section, we describe the different components of our study. Here, we discuss the network architecture, PHY layer model proposed for CR-LPWAN systems, and the experimental setup constructed to investigate the different ATTs.

3.1. CR-LPWAN-based network architecture

Every CR-LPWAN system requires a suitable network architecture for its deployment. In this section, we present a network architecture in Figure 1 that supports CR-LPWAN systems by introducing some basic network elements such as the network GW, a network server, and the IoT-based end-nodes. Essentially, we designed the network architecture in Figure 1 such that the CR components are deployed at the GW. By deploying the CR functions at the GW instead of at the end-nodes, we are able to minimize the design complexities incurred at the LPWAN end-nodes, which are often resource constrained. It is thus convenient to deploy CR technologies at the GW since most GW infrastructures often possess far more computational and physical resources than the end-nodes (ie, the sensors). Thus, the communication system benefits from deploying the ATT at the GW since the GW uses its robust computational resources in order to sense and operate the ATT. Consequently, the GW is able to effectively determine whether the channel of interest is free or occupied. If an intended channel is free for opportunistic communication, then details of the intended channel are sent by the GW to the different end-nodes for onward transmission to the end-nodes. Intuitively, this design implies that the life time of a resource-constrained end-node can be prolonged since it avoids running e ATT, thus conserving its energy resources as required in CR-LPWAN systems.

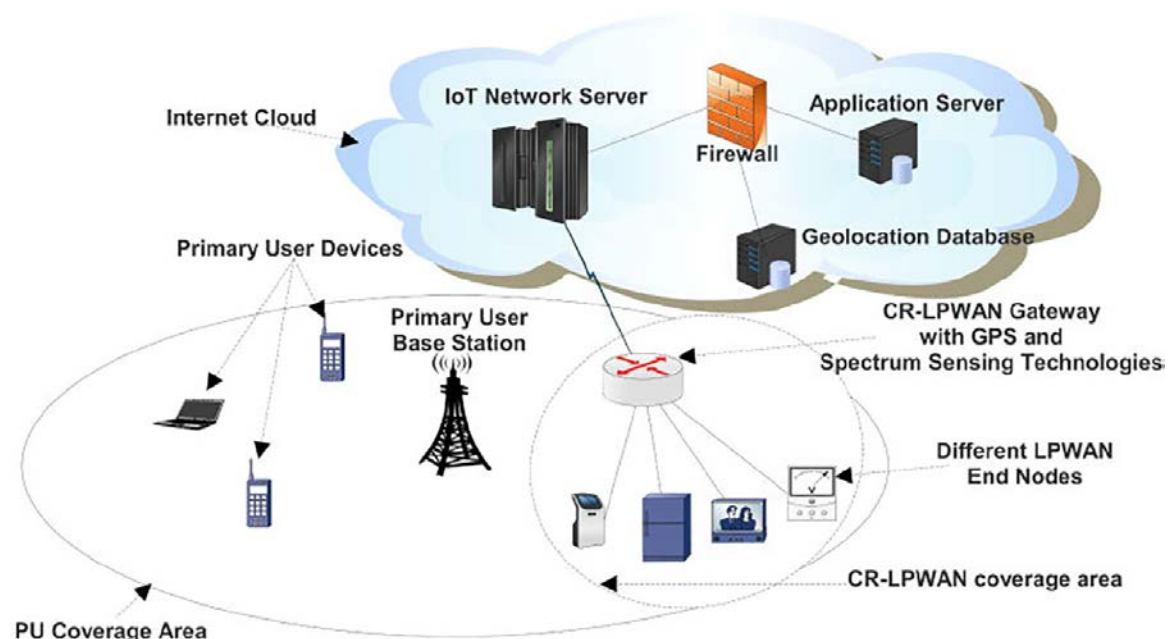


Figure 1. A network architecture depicting a CR-LPWAN gateway

Thus, when in operation, first, the CR-LPWAN GW scans its surrounding spectra in order to detect free channels (white-spaces) for opportunistic use. In some other cases, the geolocation database technology may be used to supplement spectrum sensing at the GW as discussed in Reference 7. However, our study considers the case for spectrum sensing since spectrum sensing is typically required by the IEEE 802.22 standard for CR.²⁴ In our design, the LPWAN network exists within the coverage area of at least a single PU transmitter as depicted in Figure 1. We assume that such a PU transmitter(s) works in the TV white-space (TVWS), that is, in the VHF-UHF band.

Essentially, when a free channel is detected, the CR-LPWAN GW initiates communication by broadcasting this free channel to the participating LPWAN end-nodes within the network (see Figure 1). These end-nodes may include sensors (such as in smart factories/industries) and these sensors may communicate to the CR-LPWAN GW via the identified white-space. Then, the GW is linked to an IoT network server through different application servers based on a dedicated firewall. The CR-LPWAN network model considered in our study is able to facilitate different IoT and Industrial IoT-based applications since it integrates CR at the GW instead of at the end-nodes.

3.2. PHY layer front-end model

We present a PHY layer model in Figure 2 for CR-LPWAN systems. This PHY layer model resides in the GW, which decides based on a well-chosen ATT whether PU signals are present (H_1) or not (H_0) in the sensed band.^{5, 25} Thus, based on the decision from an ATT, the GW activates the spectrum access/sharing module (see Figure 2) only if the H_0 case suffices to be true. The spectrum access/sharing module is activated in order to setup the LPWAN module toward communicating over the band. However, if the H_1 condition turns out to be true, then the spectrum mobility module will be activated to expedite quick withdrawal from the band. This command to withdraw from the band is fed to the transmission controller toward disengaging any on-going transmission process in the LPWAN module.

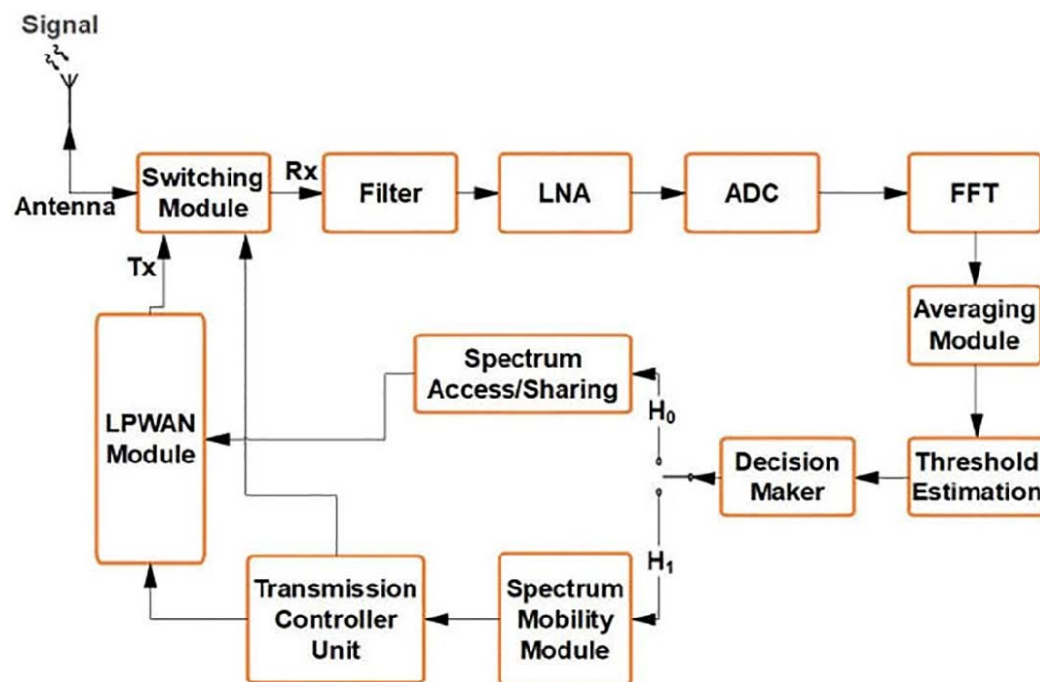


Figure 2. A PHY layer front-end model for CR-LPWAN systems

Then the GW activates the switching module (SM) (see Figure 2) based on the command received from the transmission controller so that sensing may commence again (receiving mode). The SM is a duplexer that enables a single antenna to be used for transmission as well as for signal reception. If the H_0 case persists, the LPWAN module remains active and the SM (ie, the duplexer) keeps the GW in the transmit mode.

The LPWAN module is introduced in our design to cater for the specific LPWAN PHY layer functions that are based on the proprietary nature of the different LPWAN technologies. For example, such proprietary functions may include special modulation types, different bands of operation, unique number of channels, link symmetry, adaptive data rates, and payload length. Furthermore, special MAC layer operations may include different methods for forward error correction, handover, authentication, and encryption. However, we do not discuss these LPWAN functions in this article since they are covered extensively in other documents such as in References 1 and 26.

The details concerning the individual blocks of Figure 2 are discussed as follows:

3.2.1. Antenna

Proper antenna design is critical to the success of any wireless transceiver, including CR-LPWAN systems. Striving to achieve good antenna characteristics will guarantee effective signal propagation as well as reduce the energy consumption rate of a typical CR-LPWAN system. Essentially, antenna wavelengths must match the operating frequencies of a CR-LPWAN system. Low-cost antenna technologies have been discussed in Reference 27 with focus on the design of cost efficient antennas for the 868 MHz band. The antenna design in Reference 27 considers an inverted F antenna (IFA) topology and simulation results indicate that a reflection coefficient of -6 dB in the 850 to 893 MHz band can be achieved. Lizzi et al²⁸ has also proposed an antenna miniaturization technique for IoT applications, which can be adopted for CR-LPWAN systems. They demonstrated that the overall IFA length is often responsible for the lower antenna resonance achieved in LoRa communication systems.²⁸ Thus, such similar antenna designs can be considered for use in typical CR-LPWAN systems.

3.2.2. Switching module

The SM is a duplexer that enables bidirectional transmission over a single path. The SM separates the receiving path from the transmitting path while ensuring that the CR-LPWAN GW uses a common antenna for the transceiver. Such a design has been elaborated and prototyped by Saifullah et al.^{6, 7} Nevertheless, several other LPWAN proposals often suggest that half duplex mode can also be used.^{1, 29-31} In particular, the popular LoRa SX1276 transceiver series are based on the half-duplex mode, which makes it suited for CR-LPWAN systems. Essentially, we suggest that either the half or full duplex mode can be deployed for CR-LPWAN systems depending on the application type.

3.2.3. Low noise amplifier

The low noise amplifier (LNA) amplifies the received radio frequency signal toward improving the received SNR. There are several available low-cost LNA modules that can be used in a typical CR-LPWAN system. For example, a duplex current-reused CMOS LNA with complementary derivative superposition technique was proposed for IoT purposes³² and such modules can be deployed for CR-LPWAN systems. The CR-LPWAN architecture only

requires that the LNA maintains a low-power consumption rate toward conserving and prolonging battery lifetime.

3.2.4. Filtering and down conversion

It is essential to filter and down-convert the input signal frequencies to their intermediate frequencies (IF). This process will normally be achieved by using a mixer to obtain the in-phase and quadrature components of the IF signal. Further processing of the signal can be done at either the IF or baseband level toward reducing the design complexity of the CR-LPWAN system.

3.2.5. Analog to digital converter

The analog to digital converter (ADC) converts the input signal to its digital form to present a fully digitized front end system for the CR-LPWAN system. Generally, a pair of readily available Sigma Delta ADCs can be used to perform such data conversion processes since they are typically low energy compliant.

3.2.6. Fast Fourier transformation module

The fast Fourier transformation (FFT) module computes the energy content of the input signal. This can be readily achieved using commonly available modules such as the FFT LogiCORE IP core module, which implements the Cooley-Tukey FFT algorithm in a particularly efficient manner.³³

3.2.7. Threshold estimator

The threshold estimation module computes a threshold value used to determine the presence/absence of PU signals in the band of interest. This is often a function of the noise floor, which depends further on the gain of the receiver, the matching filter, and the bandwidth. The choice of an effective threshold method will be fundamental to the success of CR-LPWAN systems, thus motivating the present study. We shall provide further details in the next section with regard to the candidate investigated ATTs.

The decision maker module may simply be a comparator, which compares the received signal strength to the estimated threshold value to determine the presence or absence of PU signals in an intended channel. The other processes involved in accessing a licensed band can be handled easily by existing proprietary LPWAN technologies such as the proprietary processes adopted in LoRa, Sigfox, and Weightless. The above details are thus presented only as an overview of our CR-LPWAN PHY layer front-end. It is envisaged that the present design will serve to inspire more sophisticated and encompassing models deployed for CR-LPWAN systems.

3.3. The adaptive threshold techniques

We investigated seven different ATTs based on the PHY layer front-end model described in Section 3.2. These ATTs include the HPA,¹⁵ MHPA,¹⁵ ROHT,^{12, 13} FOST,¹⁴ FCME,¹¹ MOA,¹⁶ and the NPAQM.¹⁷ These algorithms were considered for their simplicity, being all of $O(N)$, where N is the total number of input samples, and for their minimal control parameter sets (ie, having not more than two parameters to be fine-tuned), which makes them easy to optimize

for improved performance. These characteristics are summarized in Table 1 and these techniques are concisely described as follows:

Table 1. Summary of the different investigated ATTs

ATT	Control parameters	Time complexity	Fully autonomous	Potentials for CR-LPWAN
HPA	Descent parameter, P_{FA} rate	$O(N)$	No	Deployable for applications requiring stringent P_{FA} rates
MHPA	—	$O(N)$	Yes	Deployable for remotely situated GWs where self-reconfigurability is required
ROHT	Mean coefficient, Stopping Criterion	$O(N)$	No	Deployable for applications requiring stringent P_{FA} rates
FOST	Mean coefficient	$O(N)$	No	Deployable for applications requiring stringent P_{FA} rates
FCME	Threshold parameter, Percentage of Clean Samples	$O(N)$	No	Deployable for applications requiring stringent P_{FA} rates
NPAQM	—	$O(N)$	Yes	Deployable for remotely situated GWs where self-reconfigurability

3.3.1. HPA and mean-based HPA

The HPA and MHPA work by first generating the histogram of an input dataset, which are often the power spectral density (PSD) of the input data samples. Then, both algorithms locate the first peak in the histogram, which is generally considered to be the mean of the noise floor. Thereafter, a search is initiated in order to locate the minimum point that corresponds to the threshold value to be estimated. The end point of the search process is governed by a *descent* parameter β defined in Reference 15, eq. (5). Once computed, β is used to determine the stopping point along the slope of the histogram, which corresponds to the threshold value. The difference between the HPA and the MHPA is that the HPA uses β to determine the stopping point of the search process, which also controls the P_{FA} rate of the HPA, whereas the MHPA uses the mean of the smoothed counts per bin, obtained from the histogram, to determine the stopping point of the search process. Based on this simple difference, the MHPA is considered to be a fully autonomous method since it requires no parameter to be fine-tuned. The complete pseudocode of both algorithms are elucidated in Reference 15, sec. 3.2.

3.3.2. Recursive one-sided hypothesis testing

The ROHT receives the input PSD dataset and creates a set S belonging to the set of signals in the PSD dataset. It also creates an initial set Q belonging to the set of noise samples within the PSD dataset. Initially, the entire PSD dataset is classified as belonging to Q . Then, the ROHT iterates recursively by creating a subset of S and Q per iteration termed S_k and Q_k , respectively, where k denotes the iteration index. After every k th iteration, the ROHT computes the mean μ and SD σ of the elements in Q_k and a decision threshold γ_k is then computed per iteration as $\gamma_k = z\text{-value} \times \mu_k + \sigma_k$. Thereafter, γ_k is used to classify the dataset where samples below γ_k would belong to Q_k , whereas samples above γ_k would belong to S_k . This iterative process thus continues until a stopping criterion is satisfied, which is activated when the difference between two successive SD values is less than ϵ , where ϵ can be any small arbitrary value defined by the user. Further details about the ROHT can be found in Reference 12, sec. 3.

3.3.3. First-order statistical technique

The FOST algorithm is the simplest technique wherein the threshold γ is computed as $\gamma = h \times \mu + \sigma$, where μ and σ are the mean and SD of the input PSD dataset. Here, h refers simply to a coefficient introduced to control the magnitude of the estimated γ value, thus invariably controlling the P_{FA} rate of the algorithm. We note that the FOST and ROHT algorithms are based essentially on the same threshold function except for the recursive mechanism, which is absent in the FOST algorithm. More details about the FOST can be found in Reference 14.

3.3.4. Forward consecutive mean excision

The FCME algorithm works by iteratively classifying the input PSD dataset based on a threshold function defined as $x_q > T_{cme}$, where x_q refers to the input dataset per sample q , T_{cme} is the threshold parameter and Q is the percentage of the clean set, which defines the total number of samples within the window. Essentially, T_{cme} is calculated based on a desired P_{FA} rate defined by the user. The FCME algorithm then classifies the dataset after each iteration and the signal-free samples (ie, noise samples) are sequentially added to the clean set Q until no outlier sample is greater than the estimated threshold value. At this point, the FCME algorithm terminates and returns the estimated threshold γ to be used for signal detection. The FCME algorithm has been used extensively in the literature and further details can be found in Reference 11.

3.3.5. Modified Otsu's algorithm

The MOA is a fully autonomous method deployed to classify noise from signal samples in an input PSD dataset. Essentially, the MOA computes the histogram of the input PSD dataset and then it maximizes the between-class variance that exists between the noise and the signal subsets over several potential threshold values. These threshold values typically correspond to the different bins of the histogram. The threshold that produces the maximum between-class variance is generally defined as the optimal threshold value used for signal detection. The MOA is a modification of Otsu's algorithm and further details concerning the MOA can be found in Reference 16, sec 3.2.

3.3.6. Nonparametric amplitude quantization method

The NPAQM is also a fully autonomous method for dynamic threshold estimation.¹⁷ It works similarly to the MOA, although without requiring the need for histogram and grayscale computations as in References 13 and 16. The NPAQM adopts the first-order difference of the between-class variance computed based on the input dataset and used to determine the best threshold value for effective signal detection. Furthermore, the NPAQM boasts of an inbuilt heuristic algorithm introduced in order to detect when an input dataset contains only noise samples. This heuristic ensures that the NPAQM maintains very low P_{FA} rates under noise-only conditions. This heuristic is considered to be a major improvement of the NPAQM over other ATTs.

3.4. The experimental setup

The experimental setup designed to investigate the different ATTs is described in this section following the CR-LPWAN front-end model presented in Figure 2.

We used MATLAB to encode the candidate ATTs and then interfaced them to the USRP B200 SDR module as shown in Figure 3. The USRP B200 SDR kit was used to model the PHY layer front-end model as presented in Figure 2. The receiver of the CR-LPWAN GW was modeled physically as in Figure 3 by using the single channel B200 transceiver board to measure the electromagnetic spectrum around the local environment of the CR-LPWAN GW (ie, the setup in Figure 3). Since the USRP board measures signals within the range of 70 MHz to 6 GHz, thus, we investigated the TVWS spectra (ie, between 300 and 800 MHz) presently being considered by the Federal Communications Commission (FCC) for the deployment of CR-based technologies.²⁴ Essentially, the signals measured by the USRP B200 module were interfaced to a computer wherein processing was conducted. We subjected each ATT running in the PC to the same input dataset as measured from the USRP module in order to examine the P_D and P_{FA} rates of each technique.

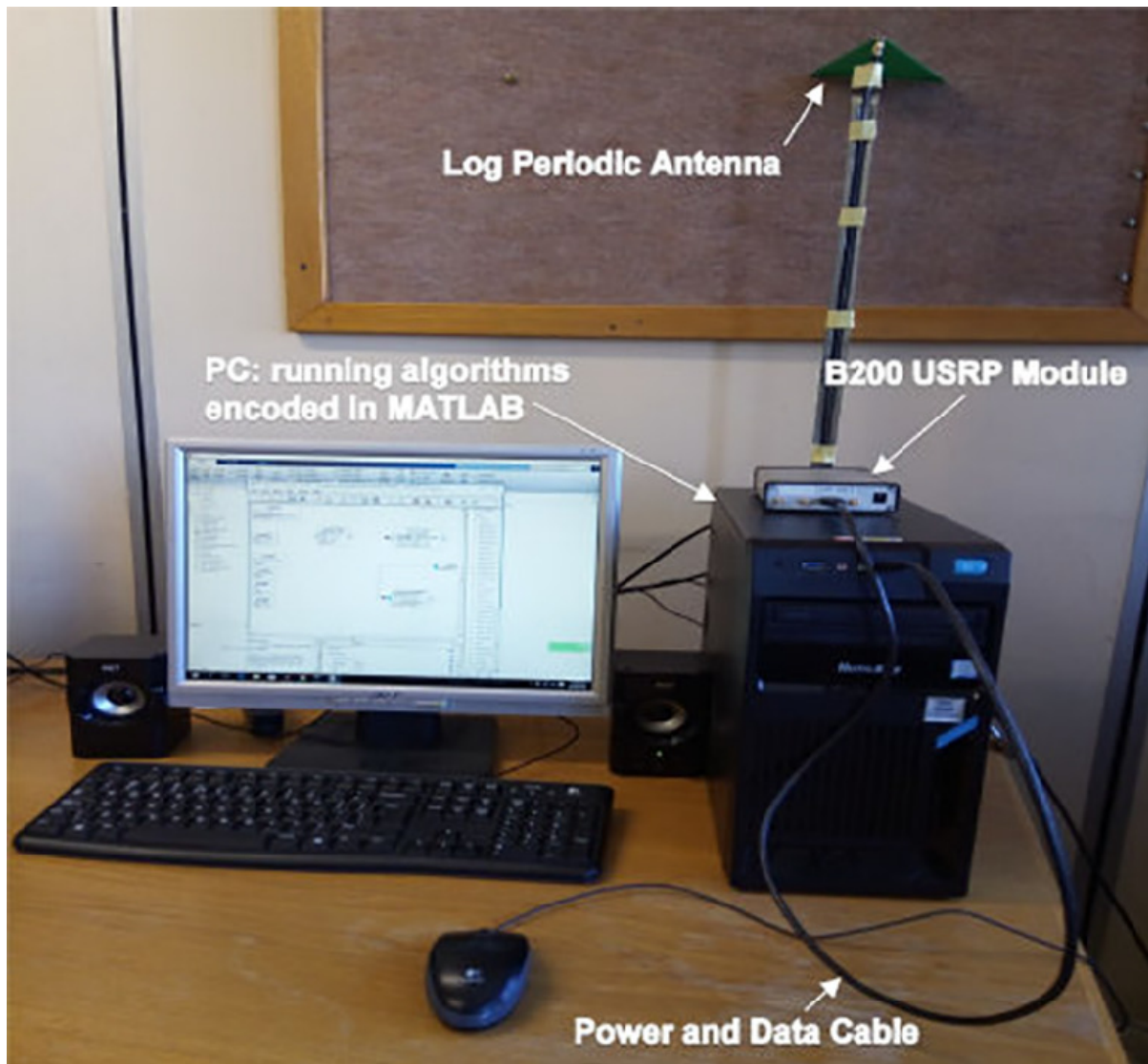


Figure 3. Experimental setup of the emulated CR-LPWAN GW

In our experiment, the B200 board and an input antenna served as part of the front-end of the emulated CR-LPWAN GW. The different ATTs investigated in this article were deployed in a PC, which served as the processing unit of the GW. We used the PC as the processor of the CR-LPWAN GW since the CR-LPWAN GW typically determines whether the sensed band

is free H_0 or not H_1 . Furthermore, the PC was considered to be a makeshift processor since we assumed that most GWs are often robust in terms of their computational, power supply, and memory resources.¹ We coupled a log periodic antenna, which has an input frequency range between 400 MHz and 6.5 GHz, to the input of the B200 board, which enabled us to properly investigate the intended VHF/UHF band for TVWS operation. In addition, the antenna has an antenna factor of between 24 and 40 dB with a typical forward gain of 6 dBi. This antenna was considered in our setup because of its good crosspolarization property, which contributes greatly toward reducing the uncertainty in the measured values. Power supply was provided from the PC to the USRP B200 board via a USB 3.0 cable through which data were also received. The power spectral of the measured signals over different bands of interest were computed prior to the threshold estimation phase.

Following the network architecture of Figure 1, it is expected that the CR-LPWAN GW operates within the coverage area of one or more PU transmitters. Thus, we modeled the presence of a single PU transmitter assumed to be transmitting within the coverage of the CR-LPWAN GW by using a similar USRP B200 module. This B200 module was interfaced to a different PC wherein the different signal types were generated. We investigated different signal types including sample sets that contained only additive white Gaussian noise (AWGN) samples, signal types based on orthogonal frequency division multiplexing (OFDM), and frequency modulation (FM) techniques. These different signal types were used to investigate different possible types of PU transmitters that may operate within the coverage area of a CR-LPWAN system. Our findings are discussed in Section 4.

3.5 Empirical method of analysis

We analyzed the performance of the candidate ATTs using the computed P_D and P_{FA} rates defined statistically as:

$$P_D = \Pr(Y(k) \geq \gamma | H_1), \quad k = 1, 2, \dots, V \quad (1)$$

$$P_{FA} = \Pr(Y(k) < \gamma | H_0), \quad k = 1, 2, \dots, V \quad (2)$$

where γ is the threshold value estimated by the specific ATT under consideration at the time, $Y(k)$ is the measured signal power, and k refers to the frequency index. Then, we computed the P_D and P_{FA} rates per dataset using Fawcett's approach.³⁴ Following Fawcett's approach, first, we obtained the ground truths of the different measured signal sets by labeling the actual signal samples in the frequency domain as ones (ie, true signal samples), and the noise samples within the same band were labeled as zeros (ie, the true noise samples). To achieve this, the signal power at each frequency index k within a sensed band was compared with the true threshold value in order to construct the ground truth that corresponds to each dataset. The actual thermal noise level in the band was used as the true threshold value in order to obtain the different ground truths per dataset. This implies that the maximum true noise value of each dataset was used as the true threshold to classify the ground truth. Thus, the ground truths were obtained from the true dynamic range of each dataset.

Consequently, the P_D and P_{FA} rates per dataset were computed as:³⁴

$$P_D = \frac{\phi}{P} \quad (3)$$

where ϕ is the number of true positives (truly detected signal samples) given that $Y(k) \geq \gamma | H_1$ and P is the total number of actual true signal samples, and

$$P_{FA} = \frac{\varphi}{N_0}, \quad (4)$$

where φ is the number of false positives (falsely detected signal samples) given that $Y(k) < \gamma | H_0$ and N_0 is the total number of noise samples. The different performance curves under different conditions are presented in Section 4. These were plotted as the P_D and P_{FA} rates against their corresponding threshold values. This presentation enabled us to clearly identify the threshold values estimated by the different techniques and to easily read-off their corresponding performance points along the graphs.

4. RESULTS AND DISCUSSION

This section discusses our findings under two main subsections, namely, the noise-only and signal-plus-noise spectra conditions. These regimes were investigated since they represent real-life conditions under which CR-LPWAN systems may be deployed. The section on noise-only conditions examines the false-alarm performance of different ATTs, which we modeled within the PHY layer of a CR-LPWAN system. Here, we considered conditions that describe both noise uncertainties and pink noise realization. The section on signal-plus-noise conditions, on the other hand, presents a number of different detection challenges to the different models, which we describe under both the microphone and the digital television (DTV) signal conditions, and under narrow and wideband sensing conditions. Our findings are discussed relative to the IEEE 802.22 standard, which states that the probability of detection P_D should be $P_D > .9$ and the probability of false alarm P_{FA} should be $P_{FA} < .1$.²⁴

A summary of the characteristics of each investigated scenario is presented in Table 2.

Table 2. Characteristics of the different investigated scenarios

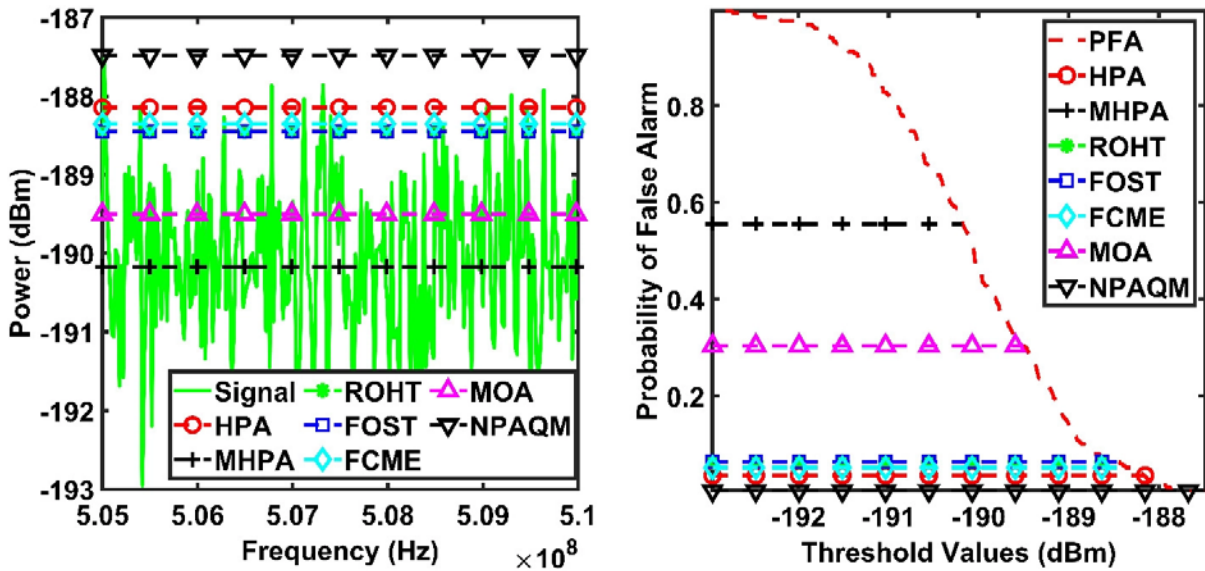
Sensing conditions	Categories	Bandwidth (MHz)	Characteristics
	Reference level	5	Spectra contained only noise samples at a peak level of -190 dBm, considered to be the reference level
Noise-only	Noise uncertainty	5	Uncertainty was introduced by increasing the reference level by 2 dB from -190 to -188 dBm
	<i>Pink</i> noise	200	Noise level slowly ramps downward from left to right over a very wide bandwidth
Signal-plus-noise	Microphone signals	5	Involving frequency modulated (FM) signals at low SNR ($=1$ dB) and high SNR ($=10$ dB)
	Digital TV signals	5	Involving OFDM signals at low SNR ($=3$ dB) and high SNR ($=10$ dB)
	Under different occupancy conditions	25 (for low occupancy) 1 (for high occupancy)	Low occupancy condition had the signal occupying less than 5% of the entire bandwidth High occupancy had the signal occupying over 80% of the entire bandwidth

4.1. Noise-only conditions

This subsection investigates how the different models would perform under increasing average spectral noise levels (noise uncertainty) as well as when the noise level ramps slowly downward (*pink* noise). These conditions can be encountered in certain real-life situations, for example, the case for *pink* noise can be experienced under conditions of wideband sensing. These conditions are important and should be examined since they are easily encountered by CR-LPWAN systems in typical IoT-based applications.

4.1.1. Noise-only spectra at a reference level (0 dB)

Figure 4A presents the noise dataset measured at the PHY layer front-end of the CR-LPWAN system. The figure displays the different threshold values estimated by the different ATTs based on an average reference noise level of -190 dBm. We considered this average reference level to be the 0 dB level and all other noise increments were conducted with reference to this 0 dB level. We present in Figure 4B only the P_{FA} performance curve since the dataset used in this experiment contained only noise samples. The P_{FA} performance of each ATT is indicated by the respective horizontal lines shown in Figure 4B. The MOA and MHPA performed least with high P_{FA} rates of $P_{FA}=.556$ and $P_{FA}=.304$, respectively (see Figure 4B). The other methods compared herewith satisfied the IEEE 802.22 standard since they achieved P_{FA} rates less than .1. The NPAQM performed best with $P_{FA}=.004$, which outperformed the next algorithm (ie, the HPA) by a P_{FA} percentage reduction rate of 88.9%. The MOA and MHPA, by being fully autonomous methods, performed poorer than the NPAQM since they lack effective methods to easily differentiate noise-only datasets from signal-plus-noise conditions. In particular, the parametrized ATTs such as the FCME, FOST, HPA, and ROHT performed well in this noise-only case since their parameters were fine-tuned a priori to a predefined P_{FA} rate based on datasets characterized by only AWGN samples.



(A) Noise-only samples showing the different threshold values

(B) P_{FA} performance

Figure 4. Noise-only spectra at a reference level (0 dB)

4.1.2. Noise uncertainty (with 2 dB increment)

We examined the case for noise uncertainty by increasing the reference noise level in Section 4.1.1 by 2 dB, resulting in a new average noise level of -188 dBm. Kindly see Figure 5A for the resulting dataset and the corresponding threshold values estimated by the different ATTs. It is observed easily in Figure 5A that the MOA and MHPA both estimated relatively lower threshold values than the other tested ATTs, which implies that they obviously suffered higher P_{FA} rates. This fact is corroborated by the corresponding P_{FA} trace of each ATT shown in Figure 5B. Here, we observe that the MOA and MHPA both achieved $P_{FA}>.2$, which violates the requirements of the IEEE 802.22 standard, albeit the MHPA only performed

better than the MOA in this case. The other algorithms tested here again satisfied the IEEE 802.22 standard, making them stable methods under noise uncertainty conditions, based on an uncertainty increment of 2 dB. Essentially, it may be argued that the parametrized algorithms considered in our experiments only performed well in this case because they were fine-tuned a priori using similar AWGN sample sets. However, since AWGN samples may not always be the case under real-life conditions, consequently, we discuss in the next subsection the case for *pink* noise-only condition, which also occurs frequently under real-life conditions.

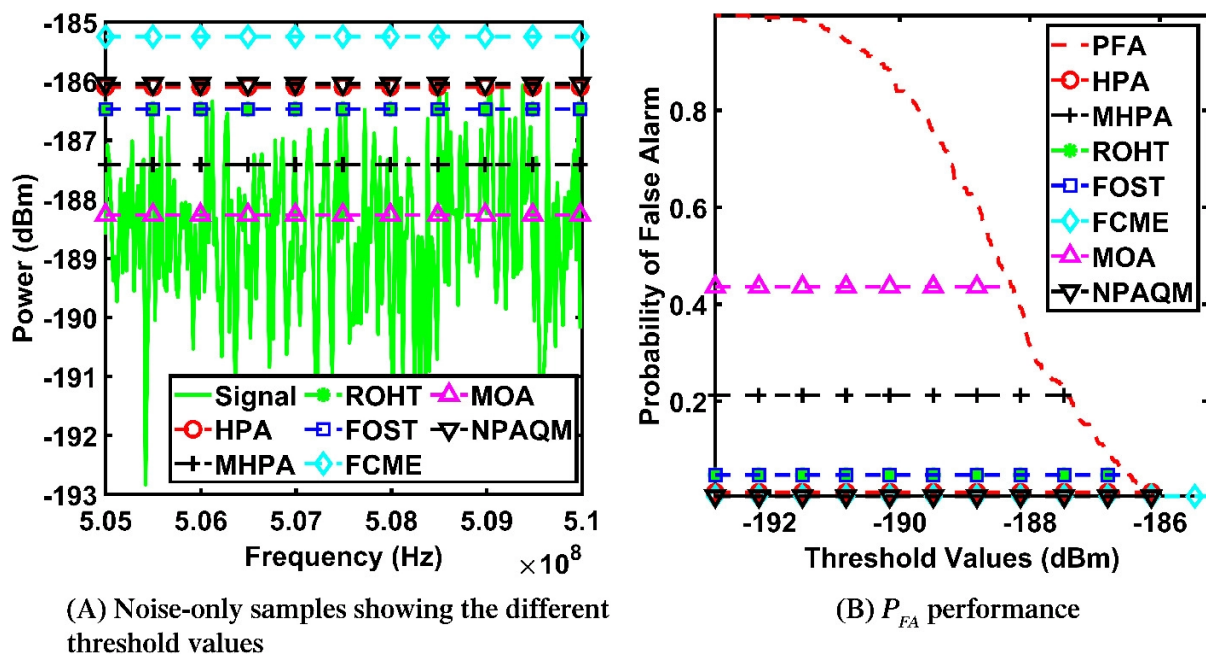


Figure 5 .Noise-only spectra demonstrating an uncertainty increment of 2 dB

4.1.3. *Pink* noise-only condition

Figure 6A shows the spectra that demonstrates *pink* noise characteristics. *Pink* noise is demonstrated in Figure 6A since the noise power level ramps slowly downward from lower toward higher frequencies. This condition may occur when CR-LPWAN systems sense relatively wide spectra as indicated in Figure 6A, that is, over a bandwidth of 200 MHz. By sensing very wide bands, the noise level may become greater at lower frequencies than at higher frequencies. Thus, following our experiments, the FCME algorithm performed best by achieving the lowest P_{FA} rate as shown in Figure 6B and the MOA being the worst performer with $P_{FA}=.6388$. Again, the other algorithms considered in our experiments achieved an average P_{FA} rate lower than .1. The FCME algorithm with $P_{FA}=.0019$ outperformed the NPAQM with $P_{FA}=.066$ by a P_{FA} percentage reduction rate of 97%.

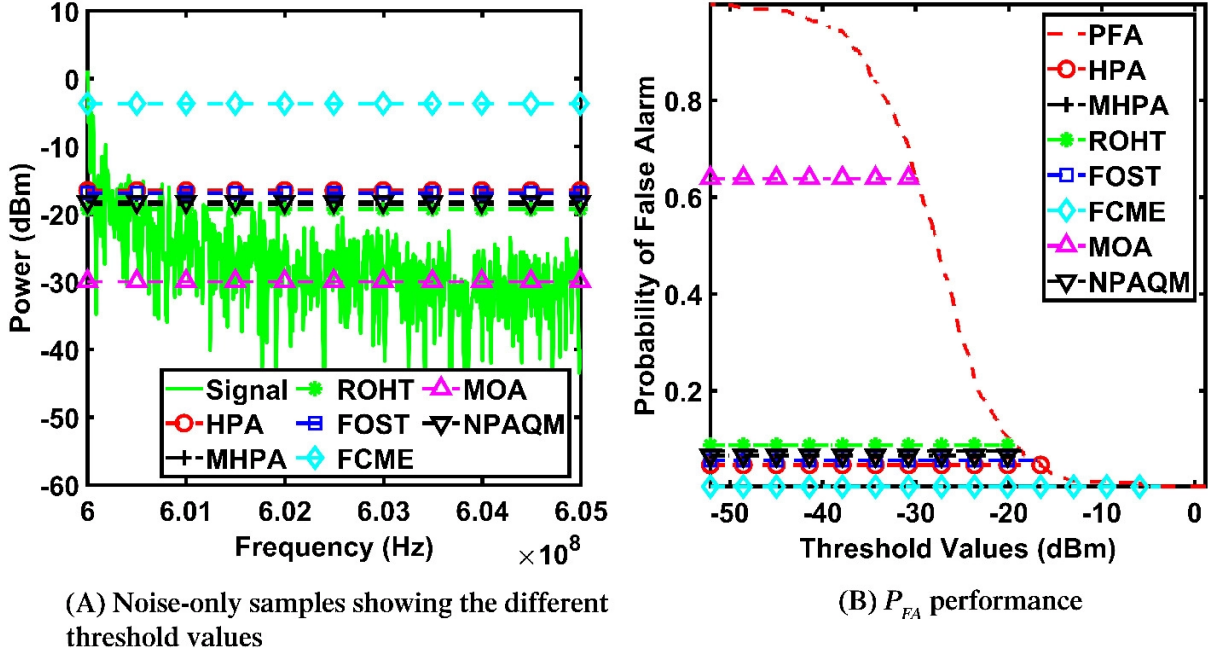


Figure 6. Performance under *Pink* noise-only spectra

In essence, our findings based on the experiments conducted and discussed above suggest that:

- The different parametrized algorithms considered in our noise-only experiments typically satisfied the IEEE 802.22 standard by providing P_{FA} rates less than .1.
- The NPAQM, being a fully autonomous algorithm outperformed other autonomous algorithms such as the MOA and MHPA under noise-only conditions. The NPAQM performed best since it adopts an effective heuristic designed to determine effectively whether a measured sample set contains noise-only samples or not.
- The success of the NPAQM suggests that fully autonomous algorithms can be deployed effectively in CR-LPWAN systems particularly for remote IoT-based applications where sensors may be required to self-reconfigure themselves.

4.2. Signal-plus-noise conditions

This subsection presents the detection performance of the different models under conditions containing different signals embedded in AWGN. Since most CR-LPWAN systems may be deployed to sense TVWS, thus, we investigated two main types of PU transmitters that reside prevalently in the TV VHF-UHF band, that is, the microphone and DTV transmitters.

4.2.1. Detecting microphone signals

Most microphone transmitters in the VHF-UHF bands typically transmit FM signals. Consequently, we examined the case for FM signals transmitted at both low- and high-SNR levels in order to analyze the performance of the different ATTs. Our findings are presented as follows:

4.2.1.1. FM signal at low SNR (1 dB)

Figure 7A presents the spectra showing the FM carrier signal and the different threshold values estimated by the different ATTs. The carrier signal is situated at 482 MHz while all other frequencies in the band contain noise-only samples. The peak noise value lies at -97.5 dBm, which serves as the ideal threshold value that maintains $P_{FA} < .0001$. Essentially, the SNR is measured by the dynamic range obtained as the difference between the peak noise power and the peak signal power at -96.5 dBm (thus being about 1 dB). The performance curves in Figure 7B,C were constructed based on this ideal threshold value and the performance of the different ATTs were measured off these curves accordingly. We see in Figure 7A that all the algorithms successfully detected the carrier signal as shown by the threshold lines that lie below the signal level. This resulted in $P_D=1$ for all algorithms as shown in Figure 7B. However, by estimating the lowest threshold value, the MOA suffered the highest P_{FA} rate as shown in Figure 7C. All other techniques considered in this experiment achieved P_{FA} rates less than .1, which conforms to the IEEE 802.22 standard. Essentially, we note that the MOA seems to perform poorly in highly noisy conditions, as it becomes difficult to effectively differentiate signal from noise samples. Thus, in the next subsection, we examine whether such findings apply or not to the case of high SNR conditions.

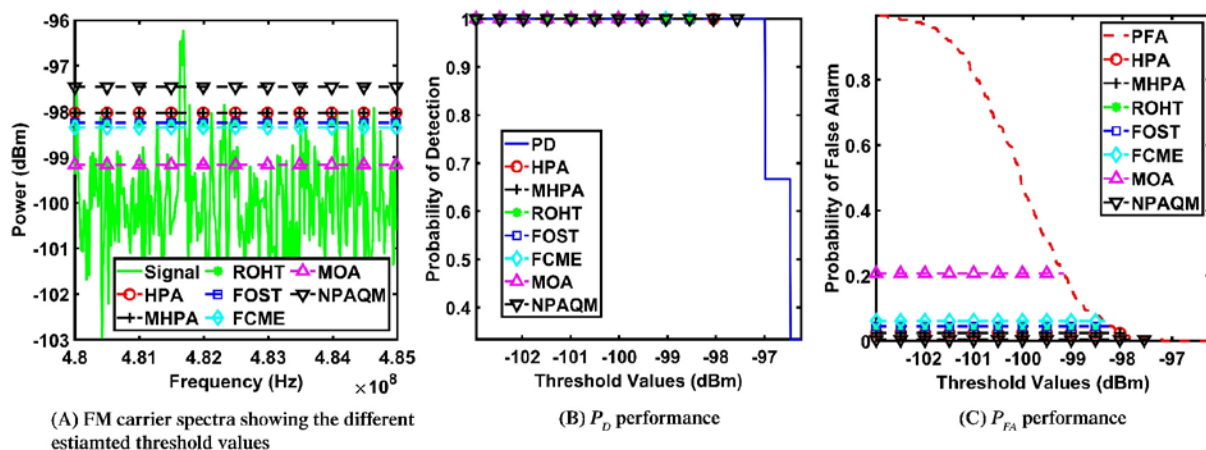


Figure 7. The case for detecting microphone carrier signal at 1 dB

4.2.1.2 FM signal at 10 dB

We increased the SNR level of the FM carrier signal to 10 dB as shown in Figure 8A to examine the performance of each algorithm. We observed that the threshold values estimated by the different algorithms were above the average noise level. This resulted in P_D rates of 1 for all the algorithms considered in our experiments (see Figure 8B) and P_{FA} rates less than .1 as seen in Figure 8C. Essentially, we can conclude that all the ATTs considered in our experiments typically satisfied the IEEE 802.22 standard when the SNR level was greater than 10 dB.

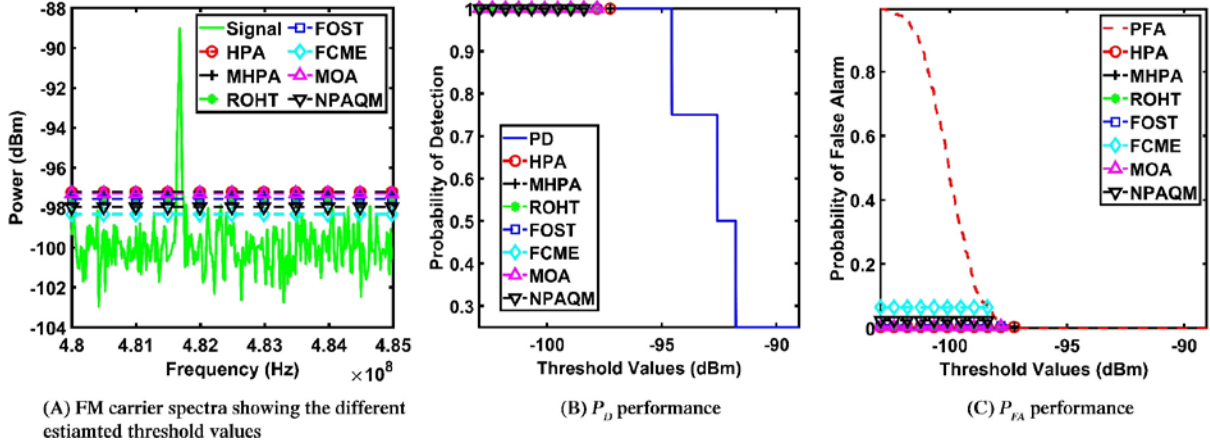


Figure 8. The case for detecting microphone carrier signal at 10 dB

4.2.2. Detecting digital TV signals

Next, we examined the case for detecting DTV signals characterized by the transmission of OFDM signals both at low and high SNR levels. Our findings are discussed as follows:

4.2.2.1. OFDM signal at a low SNR level 3 dB

Figure 9A presents the OFDM spectra and the corresponding threshold values estimated by the different ATTs. The P_D performance is shown in Figure 9B. Here, we observed that only the MOA achieved $P_D > .9$, although at the expense of a relatively high P_{FA} rate of $P_{FA} > .2$, which violates the IEEE 802.22 standard. All other algorithms considered in this experiment experienced low P_D rates below .4, albeit at low P_{FA} rates as well. A plausible explanation for this general low P_D performance may be that the OFDM spectra demonstrates typical noise-like characteristics, which may have biased these algorithms into estimating higher threshold values in a bid to keep the P_{FA} rate as low as possible. Essentially, we observed that the case for detecting OFDM at the low SNR is thus a challenge for the candidate ATTs considered in this experiment. Nevertheless, in a bid to remedy this problem, it could have been possible to reconfigure the parameters of these algorithms in order to lower their estimated threshold values. However, this is a difficult task to implement under real-life conditions since these algorithms may typically be embedded within sensors deployed in inaccessible environments. Thus, our findings suggest that detecting low SNR OFDM signals effectively is a typical problem that must be solved toward deploying effective CR-LPWAN systems. In the next subsection, we shall examine whether or not it is possible for these algorithms to detect OFDM signals easily at higher SNR levels.

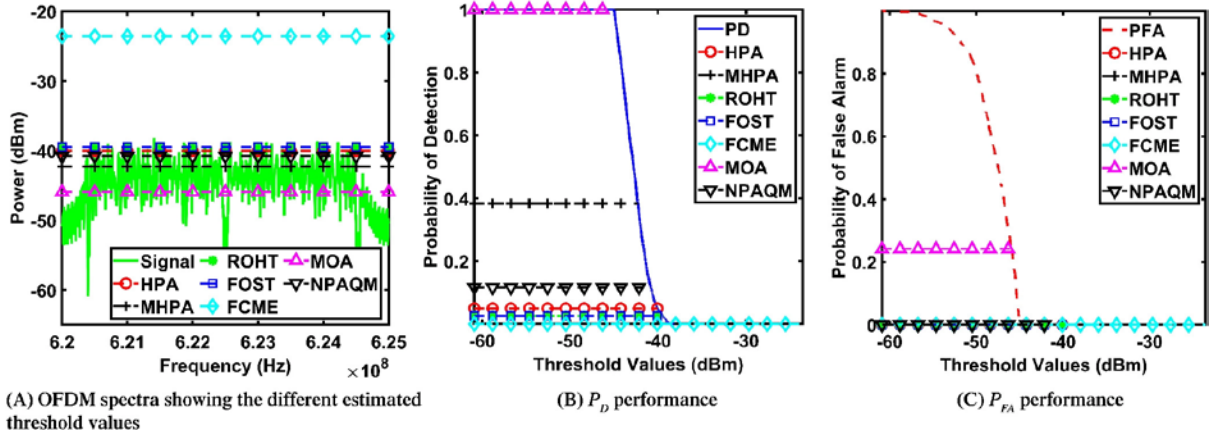


Figure 9. Detecting OFDM signals at SNR = 3 dB

4.2.2.2. OFDM signal at a high SNR level 10 dB

In this subsection, we analyze the performance of the different ATTs toward detecting OFDM signals at a higher SNR level. Figure 10A presents the sensed spectra and the threshold values estimated by the different ATTs. Following our experiment, we observed that these algorithms performed similarly to the low SNR case with low P_D and P_{FA} rates as shown in Figure 10B,C, respectively. In this case, only the MOA achieved the expected results of $P_D > 0.9$ and $P_{FA} < 0.1$, with the FCME algorithm following closely (see Figure 10B,C). Thus, it is concluded that the ATTs considered in our investigations may find it typically difficult to detect OFDM signals, a finding that requires further investigation toward the successful deployment of CR-LPWAN systems, and other CR-based technologies in general.

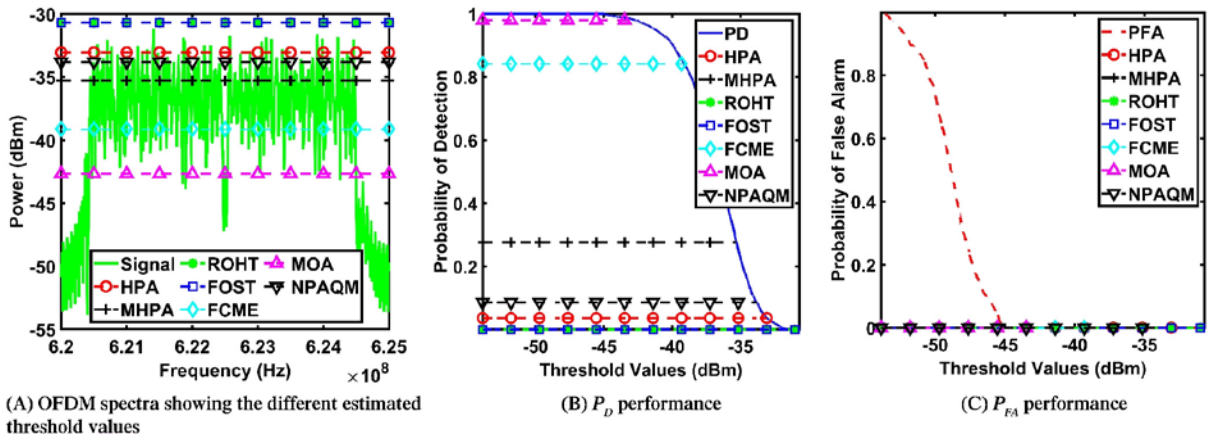


Figure 10. Detecting OFDM signals at SNR = 10 dB

4.3. Under low and high occupancy conditions

This section investigates the performance of the different ATTs under low and high occupancy conditions. Here, high occupancy condition implies that the sensed signal occupies a relatively large percentage ($\approx 80\%$) of the entire spectra, making it an approximately flat frequency response across the band. This can be encountered often under narrowband sensing situations. The low occupancy condition, on the other hand, implies that the actual signal occupies a relatively small percentage of the entire large sensed spectra ($< 10\%$). In this case, the frequency response is not often flat and this may occur under very

wideband sensing situations. In terms of bandwidth design, either of these two occupancy conditions may typically be encountered by CR-LPWAN systems under real-life situations.

4.3.1. Low occupancy condition

A bandwidth of 25 MHz was sensed and the signal occupied less than 5% of the entire bandwidth. Figure 11A shows the signal located between 606 and 608 MHz and the threshold values estimated by the different ATTs. The detection performance in Figure 11B indicates that the MOA performed poorly with $P_D=.78$, while the other algorithms achieved $P_D=1$. This good P_D performance by the other algorithms can be expected since the signal was measured at about 10 dB, making it easy to detect the transmitted signals. The MOA may have performed less in detection terms because the strong signal strength typically biased the adaptation process into estimating higher threshold values. In P_{FA} terms (see Figure 11C), we observed that all the algorithms considered in this experiment achieved P_{FA} less than .1. Thus, our findings suggest that the different ATTs may perform well even under low occupancy conditions.

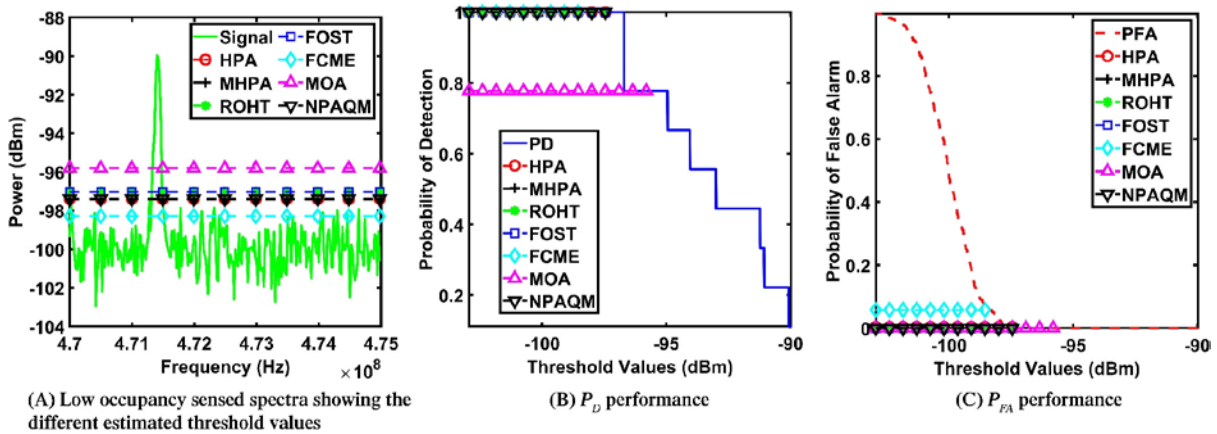


Figure 11. Performance under low occupancy sensing conditions

4.3.2. High occupancy condition

Figure 12A presents the sensed spectra and the corresponding threshold values estimated by the different ATTs. We observed that the different algorithms estimated different values, which were typically above the noise level. This implies that all the algorithms considered in this experiment achieved P_{FA} rates lower than .1 (see Figure 12C). This good P_{FA} performance can be explained noting that the spectra contained a very low noise level since most of the band contained signal samples. However, the different algorithms achieved different P_D rates, which were typically below .9 (see Figure 12B), except for the FCME and MHPA algorithms that achieved $P_D>.9$. Thus, our findings suggest that the FCME and MHPA algorithms may perform well under high occupancy conditions, particularly if the band contains at least some percentage of noise samples. However, this may not always be the case for the FCME algorithm, since it is known that the FCME algorithm performs poorly when the band contains only signal samples.³⁵ The ROHT and FOST algorithms may have performed poorly in detection terms because they depend only the mean and SD values of the dataset, which may be quite high in the highly occupied narrowband sensing case.

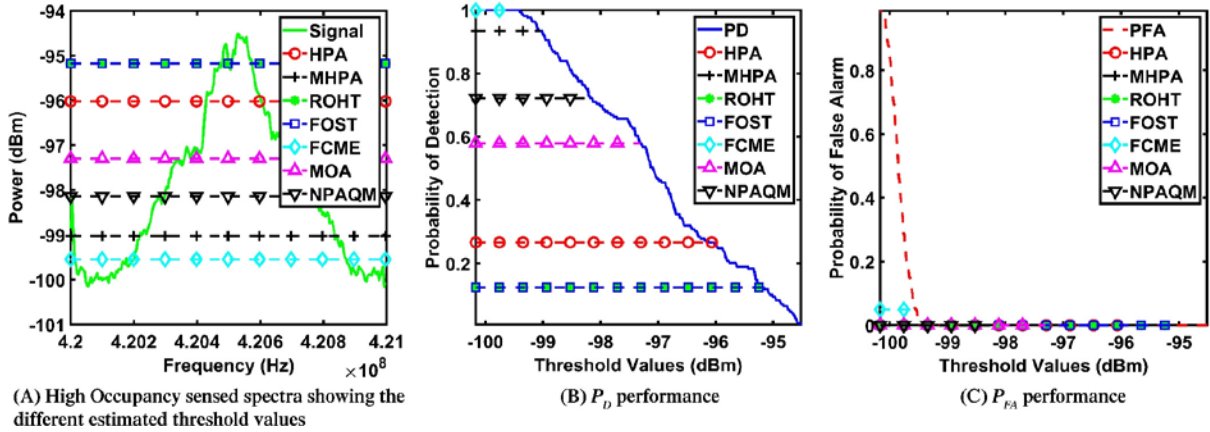


Figure 12. Performance under high occupancy sensing condition

4.4. Summary of findings

Two main sensing conditions were investigated in this study, namely, the noise-only and signal-plus-noise sensing conditions. In this section, we present a summary of our findings in Table 3 concerning the best and worst performing ATT under each sensing condition. We also postulate possible reasons why these algorithms may have performed as observed. Under the noise-only condition, particularly at the reference level, the NPAQM performed best, whereas the MHPA performed least. The use of an effective heuristic within the NPAQM may explain why the NPAQM performed best in this case. Since the heuristic of the NPAQM seeks to determine the unimodality of an input dataset, this may further explain why it was effective at discerning whether the input data contained only noise samples or not, toward minimizing its P_{FA} rate. On the other hand, the MHPA, being a fully autonomous algorithm, performed least since it uses only the mean of the input data to adjust its threshold value. In this case, this may have been an ineffective approach to deploy under noise-only conditions.

Table 3. Summary of the best/least performing ATT under different investigated scenarios

Sensing conditions	Categories	Best performer(s)	Least performer(s)
Noise-only	Reference level	NPAQM	MHPA
	Noise uncertainty	FCME, NPAQM, HPA	MOA
	<i>Pink</i> noise	FCME	MOA
Signal-plus-noise	Microphone signals	NPAQM	MOA
	Digital TV signals	MHPA	FCME
	Under different occupancy conditions	For low occupancy: all investigated ATTs except MOA For high occupancy: FCME	For low occupancy: MOA For high occupancy: FOST, ROHT

The FCME algorithm performed best under the *pink* noise condition since the first set of samples in the dataset were typically of higher power levels than other samples within the dataset. Consequently, going by the mechanism of the FCME, a higher threshold value was obviously estimated during the initial iterative process of the algorithm, thus guaranteeing a lower P_{FA} than the other investigated ATTs.

Under the signal-plus-noise conditions, we observed that the NPAQM, MHPA, and FCME achieved top performance under the microphone, DTV, and occupancy conditions, respectively. The unique approaches adopted by these different methods such as the search for unimodality by the NPAQM, the histogram partitioning by the MHPA, and an effective threshold factor may explain why these algorithms outperformed others.

5. CONCLUSION

In this article, we have investigated different adaptive threshold estimation techniques (ATT) for possible deployment in CR-based LPWANs, termed CR-LPWAN. To achieve our aim, first, we proposed a network architecture suited for CR-LPWAN systems. Our network architecture suggests that CR functionalities should be deployed at the GW toward reducing further complexities at the end-nodes, which are often resource constrained. We then introduced a PHY layer front-end model for spectrum sensing in CR-LPWAN systems. Herein, we deployed and investigated different ATTs. We constructed an experimental setup to investigate our model based on a B200 USRP module interfaced to a PC, where the different algorithms were deployed. Based on several experiments conducted under different spectra conditions, our findings suggest that there may not exist a single ATT that performs best under all sensing conditions. For example, although the FCME, NPAQM, and HPA algorithms performed well under most tested conditions, nevertheless, they may experience limited detection performance under spectra conditions containing OFDM signals. Furthermore, our findings suggest that CR-LPWAN developers may need to adopt fully autonomous methods such as the NPAQM and MHPA, particularly for IoT applications where sensors must self-reconfigure themselves, such as in military or geological remote sensing applications. Following the investigation conducted in the present article, our future works will be directed at developing real-time sensors that are embedded with these algorithms. Furthermore, we shall seek to address some specific limitations associated with some methods as disclosed by the findings of this article.

References

- ¹Raza U, Kulkarni P, Sooriyabandara M. Low power wide area networks: an overview. *IEEE Commun Surv Tutor*. 2017; 19(2): 855- 873. <https://doi.org/10.1109/COMST.2017.2652320>.
- ²Adelantado F, Vilajosana X, Tuset-Peiro P, Martinez B, Melia-Segui J, Watteyne T. Understanding the limits of LoRaWAN. *IEEE Commun Mag*. 2017; 55(9): 34- 40. <https://doi.org/10.1109/MCOM.2017.1600613>.
- ³Mekki K, Bajic E, Chaxel F, Meyer F. A comparative study of LPWAN technologies for large-scale IoT deployment. *ICT Express*. 2018; 5(1): 1- 7. <https://doi.org/10.1016/j.icte.2017.12.005>.
- ⁴Chiwewe TM, Mbuya CF, Hancke GP. Using cognitive radio for interference-resistant industrial wireless sensor networks: an overview. *IEEE Trans Ind Inform*. 2015; 11(6): 1466-1481.
- ⁵Onumanyi AJ, Abu-Mahfouz AM, Hancke GP. A comparative analysis of local and global adaptive threshold estimation techniques for energy detection in cognitive radio. *Phys Commun*. 2018; 29(C): 1- 11. <https://doi.org/10.1016/j.phycom.2018.04.008>.
- ⁶Saifullah A, Rahman M, Ismail D, Lu C, Chandra R, Liu J. SNOW: ensor network over white spaces. Paper presented at: Proceedings of the 14th ACM Conference on Embedded Network Sensor Systems CD-ROM; 2016:272-285; ACM.
- ⁷Saifullah A, Rahman M, Ismail D, Lu C, Liu J, Chandra R. Low-power wide-area network over white spaces. *IEEE/ACM Trans Netw*. 2018; 26(4): 1893- 1906.

- ⁸Chen M, Miao Y, Jian X, Wang X, Humar I. Cognitive-LPWAN: towards intelligent wireless services in hybrid low power wide area networks. *IEEE Trans Green Commun Netw.* 2018; 3(2): 409- 417.
- ⁹Dongare A, Rowe A. OpenChirp: a low- power wide-area networking architecture. Paper presented at: Proceedings of the 2017 IEEE International Conference on Pervasive Computing and Communications Workshops (PerCom Workshops); 2017:569-574; IEEE.
- ¹⁰Moon B. Dynamic spectrum access for internet of things service in cognitive radio-enabled LPWANs. *Sensors.* 2017; 17(12): 2818. <https://doi.org/10.3390/s17122818>.
- ¹¹Lehtomäki JJ, Vartiainen J, Juntti M, Saarnisaari H. Spectrum sensing with forward methods. Paper presented at: Proceedings of the MILCOM 2006-2006 IEEE Military Communications Conference; 2006:2217-2223.
- ¹²Datla D, Wyglinski AM, Minden GJ. A Statistical Approach to Spectrum Measurement Processing. Lawrence, Kansas: Information and TelecommunicationsTechnologyCenter; 2007.
- ¹³Datla D, Wyglinski AM, Minden G. A spectrum surveying framework for dynamic spectrum access networks. *IEEE Trans Veh Technol.* 2009; 58(8): 4158- 4168. Crossref Web of Science@Google ScholarCheck for full text via OCLC
- ¹⁴Gorcin A, Qaraqe KA, Celebi H, Arslan H. An adaptive threshold method for spectrum sensing in multi-channel cognitive radio networks. *17th IEEE International Conference on Telecommunications (ICT)* 2010: 425–429. <https://doi.org/10.1109/ictel.2010.5478783>
- ¹⁵Onumanyi AJ, Abu-Mahfouz AM, Hancke GP. Histogram partitioning algorithms for adaptive and autonomous threshold estimation in cognitive radio-based industrial wireless sensor networks. *Trans Emerg Telecommun Technol.* 2019; 30(10): 1- 15. <https://doi.org/10.1002/ett.3679>.
- ¹⁶Onumanyi AJ, Onwuka EN, Aibinu AM, Ugweje OC, Salami MJE. A modified Otsu's algorithm for improving the performance of the energy detector in cognitive radio. *AEU-Int J Electron Commun.* 2017; 79: 53- 63. <https://doi.org/10.1016/j.aeue.2017.04.013>.
- ¹⁷Onumanyi AJ, Abu-Mahfouz AM, Hancke GP. Amplitude quantization method for fast and autonomous threshold estimation in cognitive radio networks. *Under Rev Pervas Mobile Comput.* 2019.
- ¹⁸Dubey RK, Verma G. Improved spectrum sensing for cognitive radio based on adaptive double threshold. *Int J Emerg Trends Electr Electron (IJETEE).* 2015; 11(2): 1- 6.
- ¹⁹Avila J, Thenmozhi K. Adaptive double threshold with multiple energy detection technique in cognitive radio. *Res J Appl Sci Eng Technol.* 2015; 10(11): 1336- 1342.
- ²⁰Bagwari A, Tomar GS. Two-stage detectors with multiple energy detectors and adaptive double threshold in cognitive radio networks. *Int J Distrib Sens Netw.* 2013; 2013: 1- 9. <https://doi.org/10.1155/2013/656495>.
- ²¹Malafaia D, Vieira J, Tomé A. Adaptive threshold spectrum sensing based on expectation maximization algorithm. *Phys Commun* 2016; 21: 60– 69. <https://doi.org/10.1016/j.phycom.2016.10.004>
- ²²Wang N, Gao Y, Cuthbert L. Spectrum sensing using adaptive threshold based energy detection for OFDM signals. IEEE International Conference on Communication Systems (ICCS); 2014:359-363.
- ²³Singh A, Bhatnagar MR, Mallik RK. Threshold optimization of a finite sample-based cognitive radio network using energy detector. *EURASIP J Wirel Commun Netw.* 2013; 2013(1): 165.
- ²⁴IEEE802.22. Enabling broadband wireless access using cognitive radio technology and spectrum sharing in white spaces. *IEEE 80222 Working Group on Wireless Regional Area Networks.* 2011; 1- 30.

- 25 Onumanyi AJ, Onwuka EN, Aibinu AM, Ugweje OC, Salami MJE. A real valued neural network based autoregressive energy detector for cognitive radio application. *Int Scholarly Res Notices*. 2014; 2014: 1- 11. <https://doi.org/10.1155/2014/579125>.
- ²⁶ Sinha RS, Wei Y, Hwang SH. A survey on LPWA technology: LoRa and NB-IoT. *ICT Express*. 2017; 3(1): 14- 21. <https://doi.org/10.1016/j.icte.2017.03.004>.
- ²⁷ Pham C, Ferrero F, Diop M, Lizzi L, Dieng O, Thiaré O. Low-cost antenna technology for LPWAN IoT in rural applications. Paper presented at: 2017 7th IEEE International Workshop on Advances in Sensors and Interfaces (IWASI); 2017:121-126; IEEE.
- ²⁸ Lizzi L, Ferrero F, Monin P, Dancheski C, Boudaud S. Design of miniature antennas for IoT applications. Paper presented at: Proceedings of the 2016 IEEE 6th International Conference on Communications and Electronics (ICCE); 2016: 234-237; IEEE.
- ²⁹ Akpakwu GA, Silva BJ, Hancke GP, Abu-Mahfouz AM. A survey on 5G networks for the internet of things: communication technologies and challenges. *IEEE Access*. 2017; 6: 3619-3647. <https://doi.org/10.1109/ACCESS.2017.2779844>.
- ³⁰ Accettura N, Medjiah S, Prabhu B, Monteil T. Low power radiolocation through long range wide area networks: a performance study. Paper presented at: Proceedings of the 2017 IEEE 13th International Conference on Wireless and Mobile Computing, Networking and Communications (WiMob); 2017:1-8
- ³¹ Thomas T. LoRa, LoRaWAN, and the challenges of long-range networking in shared spectrum. *Cognitive Radio Platform NL*. 2015; 1: 1- 10.
- ³² Dai R, Zheng Y, He J, Kong W, Zou S. A duplex current-reused CMOS LNA with complementary derivative superposition technique. *Int J Circuit Theory Appl*. 2017; 45(1): 110- 119.
- ³³ Vivado DS. Logicore IP Fast Fourier Transform v9. 0. LogiCORE IP Product Guide, Xilinx; 2017:1-99.
- ³⁴ Fawcett T. An introduction to ROC analysis. *Pattern Recogn Lett*. 2006; 27(8): 861- 874.
- ³⁵ Lehtomaki J, Vartiainen J, Vuohtoniemi R, Saarnisaari H. Adaptive FCME-based threshold setting for energy detectors [Invited Paper]. Paper presented at: Proceedings of the 4th International Conference on Cognitive Radio and Advanced Spectrum Management; 2011; Barcelona, Spain